PERGAMON

Journal of Atmospheric and Solar-Terrestrial Physics 60 (1998) 1695–1705

Journal of ATMOSPHERIC AND SOLAR-TERRESTRIAL PHYSICS

Monte-Carlo simulations of proton aurora

S.A. Synnes[1], F. Søraas, J.P. Hansen*

Department of Physics, University of Bergen, Allegt. 55, N-5007 Bergen, Norway

Received 30 March 1998; received in revised form 24 September 1998; accepted 29 September 1998

Abstract

The spreading of a proton beam in the upper atmosphere is calculated based on Monte-Carlo simulations. The transport of the atoms is modelled in a magnetic field with dipole strength. Neuralisation, ionisation and excitation mechanisms of the incoming particles are included from collision cross-sections of protons and hydrogen with an effective N_2 atmosphere. Assuming an isotropic pitch angle distribution for the incoming protons, their spreading in the upper atmosphere and the return flux of the charged and neutral component of the hydrogen beam has been calculated. Depending on energy and the tilt angle of the magnetic field about 10% of the incoming particles return from the atmosphere as ENA (Energetic Neutral Atoms). The ENA returning from the atmosphere show a source region below 500 km for the incoming high energy protons. For low energy protons, the ENA originate mainly from two different regions, one around 700 km and the other at 400 km altitude, reflecting their sensitivity to several charge exchange processes.

1. Introduction

When Vegard first detected hydrogen emissions in auroral spectra in 1939, he concluded that these emissions must be due to "showers of hydrogen or to a kind of hydrogen-radiation occasionally coming from the Sun" (Vegard, 1939). Later on it was established that the emission lines were Doppler shifted (Vegard, 1948; Gartlin, 1948, 1950, 1951; Meinel, 1951) and it was established that hydrogen had come into the atmosphere as high velocity protons. The first in situ measurements of the incoming protons was made by Davis et al. (1960), flying a rocket into an aurora. Since then, protons have been measured by numerous rockets and satellites, and it is found that the protons are a persistent feature of the auroral precipitation although most often carrying less energy into the upper atmosphere than electrons. Due to the charge exchange processes, the proton beam entering the atmosphere will spread over a large spatial area. This spreading is energy and pitch angle dependent, and it also depends on the dip angle of the magnetic field. Chamberlain (1954 a, b) pointed out that the auroral hydrogen Doppler profile could give important information about the energy and angular distribution of the incoming protons, and he developed a theoretical foundation for such studies (Chamberlain, 1957; Omholt, 1956; Tuan, 1962; Kozelov and Yurova, 1991; Kozelov and Ivanov, 1992). Recently, calculations of proton and electron precipitation based on hydrodynamic transport equations have been performed by Galand et al. (1997) and Decker et al. (1996) who also compared this approach with Monte-Carlo simulations.

In all these works, apart from the one by Kozelov, parallel magnetic field lines were assumed. Thus the effect of increasing pitch angles of the protons as they spiral into the atmosphere along converging field lines could not be taken into account. Eather and Burrows (1966), however, calculated hydrogen line profiles in a dipole field. They showed that, for an isotropic pitch angle distribution, the profiles would be very similar to those calculated by Chamberlain's theory, with the addition of a small 'red shift' component due to emission from particles that had been reflected magnetically upwards. This 'red shift' was, however, not enough to account for the measured red shift in the Doppler profiles. In their calculations Eather and Burrows (1966) did not include the contribution to the Doppler profile from Energetic Neutral Atoms (ENA) moving out of the atmosphere

* Corresponding author. Tel.: 0047 55 582713; fax: 0047 55 589440; e-mail: jenpetter.hansen@fi.uib.no

[1] Present address: Norwegian Defence Research Institute, WM, Po Box 25, N-2007 Kjeller, Norway.

S1364–6826/99/$ - see front matter
PII: S1364-6826(98)00107-2

and emitting 'red shifted' photons for an observer at the ground. Since the first detection of ENA coming from the Earth's magnetosphere by Roelof et al. (1985), there has been an increasing interest in the detection of ENA. The ENA move in a straight line from the source and can thus image some of the physical processes taking place in the magnetosphere and in the upper atmosphere at auroral latitudes. ENA are now being measured in the magnetosphere by the POLAR satellite and have given new information on the build up and decay of the ring current (Spence and Blake, 1997). Søraas and Aarsnes (1996) have measured the ENA in and near a proton arc using a high flying rocket. From the measurements the location of the arc was remotely determined. The ASTRID satellite has also measured ENA at low altitudes (Norberg et al., 1995). The proton aurora is a potential intense source of ENA and it is of interest to evaluate the escape flux of ENA from this source. It is important to know the contributions to the ENA flux both from charge exchange processes in the magnetosphere and in the auroral region. In the present paper the spatial distributions of both neutral and charged particles are calculated in the altitude range from 1000 km down to the altitude where the particles are stopped in the atmosphere. These calculations are done at different local pitch angles, and results referring to 300 km altitude are presented. The spatial distribution of Hα emissions due to the spreading proton beam is presented, and the upper atmosphere source of ENA is determined for several energies and magnetic dip angles. In Section 2 the model is described and compared to earlier calculations. Results are shown in Section 3 followed by conclusions in Section 4.

2. Simulation model

The protons are assumed to have an initial isotropic pitch angle distribution over the upper hemisphere and fixed initial kinetic energy. An isotropic pitch angle distribution is in accordance with rocket and satellite measurements in the proton aurora (Søraas et al., 1974; Lundblad et al., 1979).

Isotropic pitch angle intensity, $I(\alpha) = I_0$, and taking into account only particles passing a point at 1000 km altitude on a magnetic field line leads to a distribution in the number of initial particles with given pitch angle α, $N(\alpha) = I_0 2\pi \sin(\alpha)\cos(\alpha)$. Here the z-axis is parallel with the magnetic field. For each energy in the range 1–100 keV between 10^5 and 10^6 protons are simulated depending on the number needed to produce smooth final distributions. Each proton is tracked in the atmosphere from an initial altitude of 1000 km until it reaches the near-zero energy of 100 eV, or until it passes the 1000 km height in upward motion and thus leaves the region of interest. Approximating the magnetic field strength with a dipole, the field depends on the height, h, as

$$B(h) = B_0\left(\frac{Re}{h+Re}\right)^3, \tag{1}$$

where B_0 is the magnetic field strength at ground level, and Re is the earth radius (6370 km). The pitch angle α_f at height h is then calculated from the first adiabatic invariant of the Hamilton–Jacobi variable J_1,

$$J_1 = \frac{\sin^2(\alpha_i)}{B_i} = \frac{\sin^2(\alpha_f)}{B(h)} \tag{2}$$

The pitch angle α_f is recalculated according to this relation for every km of vertical motion or after every collision if a collision occurs first. Between collisions the charged particles are bound to the magnetic field lines with gyration radius, r_c. At auroral heights, r_c (1 keV) $\approx$ 100 m and r_c (100 keV) $\approx$ 100 m. If a proton is neutralised by electron capture it will follow a straight line trajectory determined by the velocity vector before the collision. Examples of the trajectory histories of simulated particles are shown in Fig. 1 pertinent to a magnetic dip angle of 20°. The left panel shows the trajectories of ten initially low energy (2 keV) protons, and in the middle panel the trajectories of more energetic protons (100 keV) are shown. The higher energy beam in the middle panel exhibits a much more focused behaviour and the charge exchange processes starts at significantly lower heights than for the 2 keV protons. The 2 keV protons spread over a horizontal distance of several hundred km, while the 100 keV protons spread around 50 km in horizontal distance. The right panel shows the trajectories of 1000 simulated protons at 2 keV initial energy and having an isotropic pitch angle distribution, indicating that some ENA, having a northward velocity component and a pitch angle near 90°, move out of the atmosphere.

Apart from defining the magnetic field, the two main ingredients in the simulation model are the specification of the atmosphere in which the protons lose energy and the collision model specifying the allowed energy and charge transfer mechanisms. We adopt the atmosphere model defined by the U.S. Standard Atmosphere (Hedin, 1987) (exosphere temperature = 1200 K). From these data an effective N_2 atmsophere defined by the summed densities of N_2, O_2 and 60% O are obtained. This approximation relies on the assumption that the collision cross sections of O_2 and N_2 are equal, justified rather well in Andersen and Zieger (1977), Rudd et al. (1983) and Yousif et al. (1986). For p and H collisions with O, we have not been able to find any published values for the cross sections. In order to include to a first approximation the effect of collisions with oxygen we have used the same atomic/molecular ratios as can be extracted from collisions between p and atomic and molecular hydrogen.

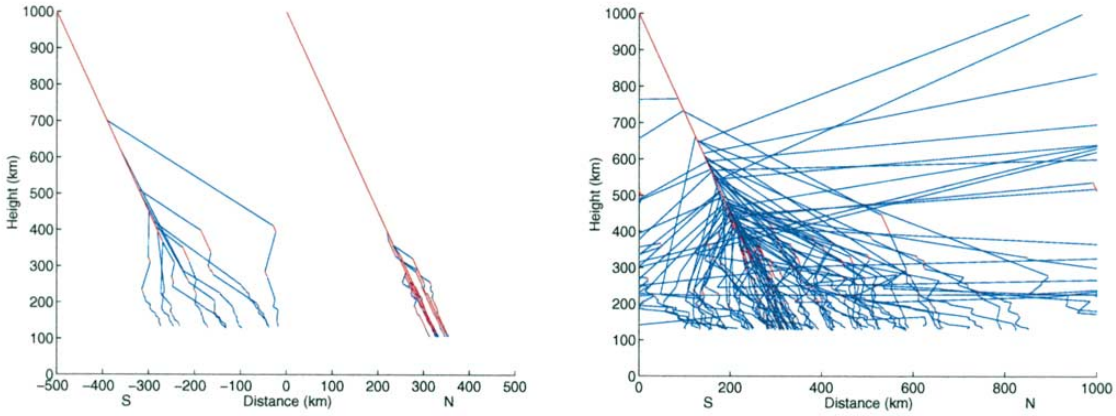

Fig. 1. Trajectories of particles entering the atmosphere at 20° magnetic inclination. Left panel: pitch angle 30° at 1000 km, 10 particles with $E_P = 2$ keV initially from 500 km to the South and 10 particles with $E_P = 100$ keV at 1000 km. Right panel: trajectories of 1000 particles with isotropic pitch angle distribution, $E_P = 2$ keV. The initial point of entry is here 1000 km for all particles.

From Kerby et al. (1995) we find $\sigma_a/\sigma_m \approx 0.6$ for the cross sections for ionisation in the energy range 20–200 keV. At these energies ionisation is most important so we employ this ratio for all total collision cross sections between atomic and molecular oxygen. We use the collision cross sections for p and H collisions with N_2 given by Kozelov and Yurova (1991) and Kozelov and Ivanov (1992).

The probability for collision involving a reaction for one single particle after passage of n atmosphere particles is exponentially distributed,

$$P(n) = \frac{\sigma}{A} e^{-n\sigma/A} \tag{3}$$

where A is unit area and σ is the total reaction cross section. The number of atmospheric particles which the projectile has passed before a reaction actually occurs can thus be drawn from a uniformly distributed random number, R, between 0 and 1, according to

$$N_{\text{coll}} = \frac{-\ln(R)}{\sigma} \tag{4}$$

The proton or hydrogen atom propagates down/upwards until this number of passed particles has been reached and a state change of the projectile takes place.

Ideally the cross section for all relevant excitation processes and the corresponding projectile energy loss for each channel should be used. This would, however, require a much more detailed knowledge of the collision processes and also make the collision algorithm rather complex. Therefore, the mean excitation energy is used for calculation of the energy loss. An exception is the energy loss of the cross sections leading to Hα emission which is treated exactly since the production of the spatial distribution and intensity of these spectra is a main result of the simulations.

For charge transfer and ionisation the total cross sections for these processes are used. For charge transfer the energy loss is also modified by the acceleration of the captured electrons. At 10 keV proton energy and above, the most important energy loss mechanism is ionisation of atmosphere particles. The mean kinetic energy of these electrons as a function of the kinetic energy of the projectile is found from the energy and angular distributions of the electrons in Rudd et al. (1971; 1979) and Toburen (1971).

The validity of the numerical interpretation is controlled by calculating the stopping cross section for p/H in N_2 and comparing it with the mean experimental value for this stopping cross section in Andersen and Zieger (1977). The stopping cross section is the stopping power (energy loss per distance) in a given gas, divided by the density of the gas. Hence, this quantity is independent of the particle density. Comparing the stopping cross sections with the experimental data in Fig. 2, rather good agreement is found between the calculated and experimental values. The solid line shows our calculations and the circles correspond to the experiments. The calculations of the high energy values are dominated by the unknown energy loss to electrons during ionisation. This is indicated by the dashed line which shows the result when this energy loss is not included. Below 20 keV excellent agreement is achieved; between 20 keV and 150 keV, the calculated values are somewhat lower than the experimental ones, and at high energies the calculated values are larger than the experimental ones. However, considering the typical 30% uncertainty of the experimental cross sections and the relatively crude treatment

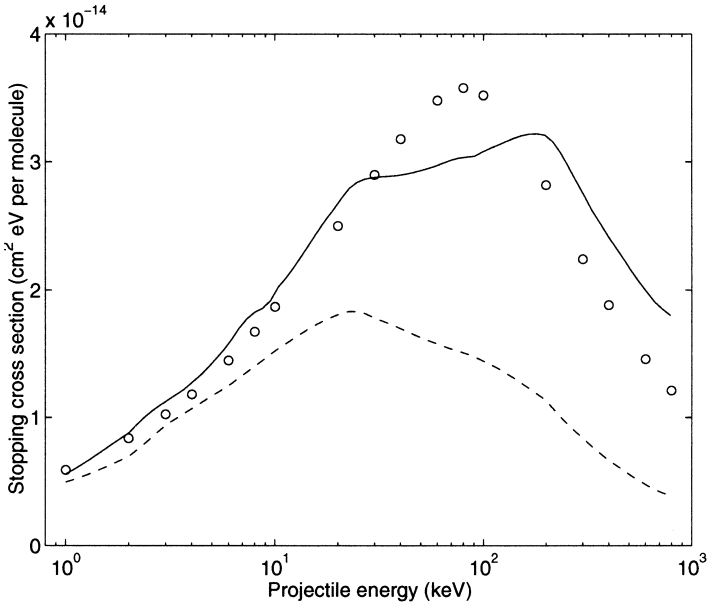

Fig. 2. H/p–N_2 stopping cross section compared with experimental data from Andersen et al. (1977) (circles). Solid line: calculations including electron energy loss. Dashed line: calculations without electron energy loss.

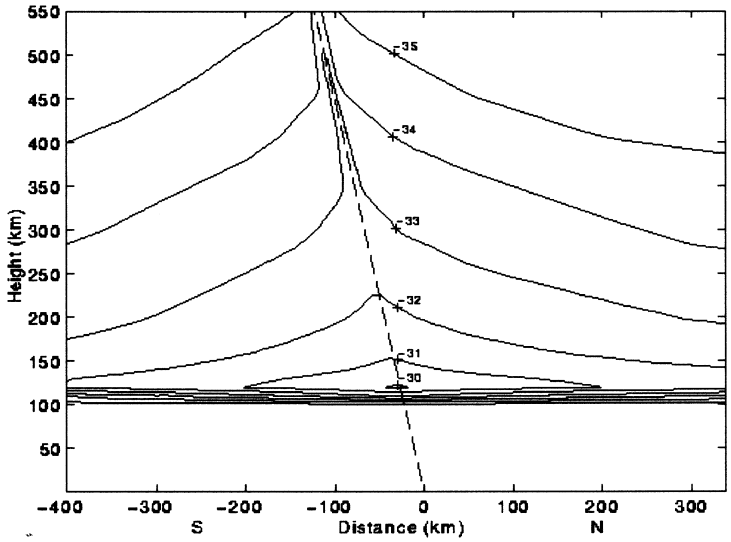

Fig. 3. The North–South and altitude distribution of Hα emissions from a proton aurora with large extension East–West and short extension North–South. The unit is log(erg/cm^3), for direct comparison with Davidson (1965). The magnetic tilt angle is 10°.

of the energy loss for the various collision channels in our model, the overall agreement seems very satisfactory.

3. Results

In Fig. 3 a contour plot for the intensity of Hα emission is shown with contour lines similarly to Davidson (1965). The relative spatial intensity distribution for the Hα emission is approximately the same for the two simulations. The emission is distributed almost symmetrically with respect to the magnetic field, but with the intensity slightly further to the North than to the South due to the tilt of the magnetic field. This close resemblance between the two simulations indicates that the spreading of the protons in the atmosphere is handled well in the two models. The absolute intensities differ, however; the intensities in Davidson's calculations are approximately

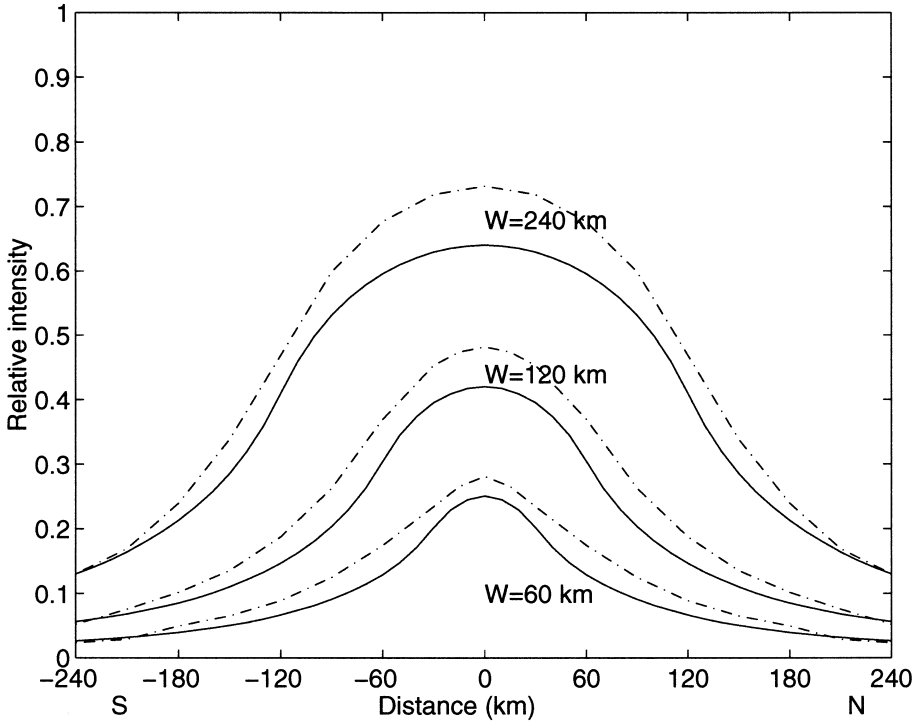

Fig. 4. North–South distribution of protons/neutrals at 300 km from proton arcs with different half-widths (W). The relative intensity is related to the intensity inside the arc at high altitudes. Full curve: our results, dash–dot curve from Inglesias and Vondrak (1974).

10% of our intensities (Synnes, 1996). This is probably due to Davidson's assumption that the cross section for Hα emission in H–N_2 collisions could be approximated by the cross section for Hα emission from the projectile in H–H collisions. Later experimental and theoretical studies have shown that the cross section for Hα emission in H–N_2 collisions is from 2 times larger at 10 keV to 20 times larger at 1 keV (Kozelov and Yurova, 1991; Kozelov and Ivanov, 1992).

A second comparison with previous work is performed with Inglesias and Vondrak (1974). Thy applied a model originally developed by Johnstone (1972) for calculation of the effect of the proton beam spreading in the atmosphere. This model only considers the length of the distance traversed in the first neutral segment and the spreading of the protons is assumed to be dominated by this distance. As seen from Fig. 4 the agreement is excellent, with less than 10% deviation between the Inglesias and Vondrak model and our model at any height. The small discrepancy between the two calculations could be caused by their neglect of mirroring particles, making their values somewhat higher than ours.

Having performed these comparisons, it appears that our simulations give a correct description of the charge exchange spreading of energetic protons in the upper atmosphere. Using a projectile energy of 10 keV and varying the angle between the magnetic field and the vertical (γ), the spreading to the North and South of the initial magnetic fieldline is calculated for a height of 300 km, and the results are shown in Fig. 5. The spreading of the beam, both the neutral and the charged component, is seen to be symmetric for a vertical magnetic field (upper left-hand panel). Particles with pitch angles close to 0° have a vertical motion, and are not spread, while particles with pitch angles closer to 90° will have a large horizontal component, resulting in a significant spreading to the North and South of the initial position. Increasing the angle between the magnetic field and the vertical gives a smaller horizontal spreading to the South and a more extended spreading to the northward direction, both in altitude and in latitude. This is particularly true for particles with pitch angles near 90°.

In Fig. 6 the beam state and the North–South/pitch angle distribution of 10 and 100 keV hydrogen at 300 km altitude are shown for a tilt angle of 10°. The figure consists of four panels; the two left ones refer to 10 keV, the charged component at the top and the neutral component at the bottom. On the right side of the figure similar information referring to 100 keV hydrogen is shown. The neutral state dominates for energies below 35 keV, and the charged state for higher energies. At 100 keV, about 80% of the particles are charged, and the spreading (due to neutral segments) is consequently small. For energies above 150 keV, the charged fraction

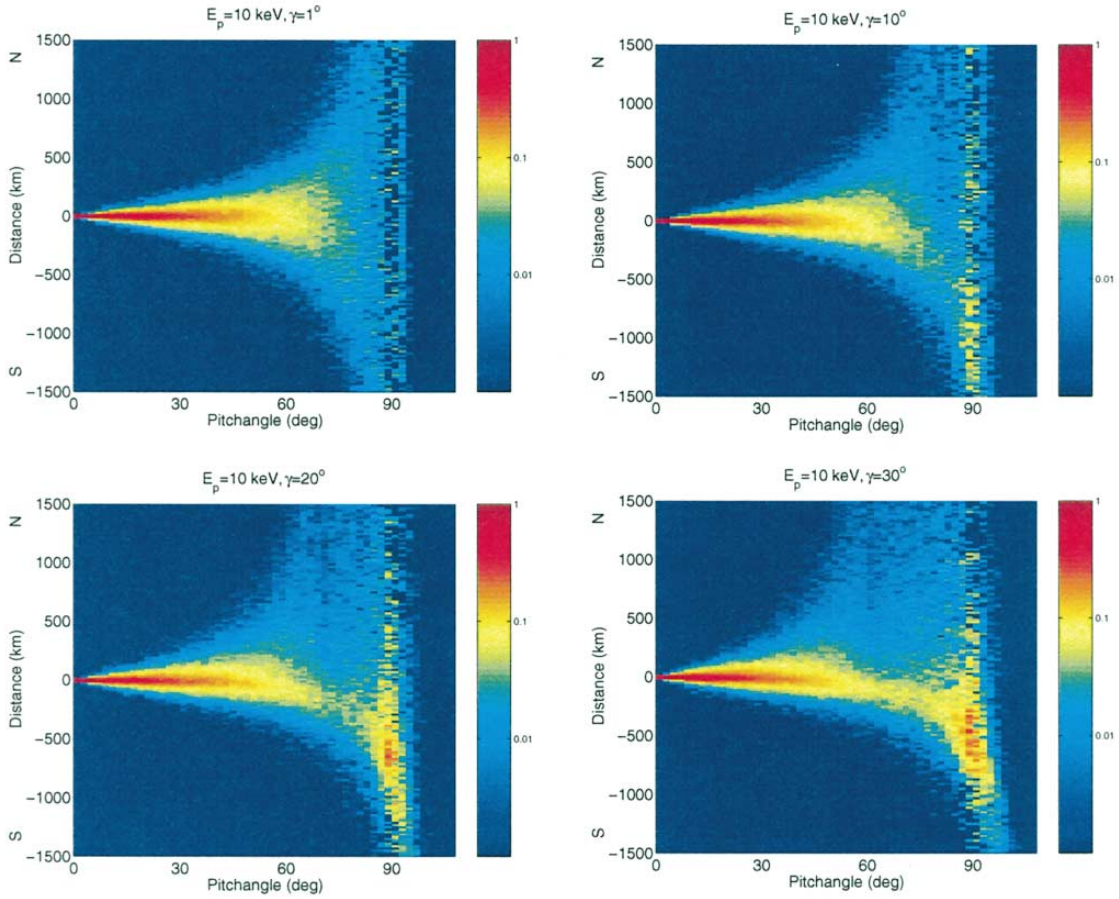

Fig. 5. The pitch angle distribution (erg/cm^3) for protons/hydrogen at 300 km altitude (mean particle energy 9.7 keV) as a function of the horizontal distance from an arc with a half width of 30 km. Four magnetic inclinations, 1, 10, 20 and 30°, are considered and the initial proton energy is 10 keV.

dominates completely, and the energy above 150 keV is lost within a few gyration radii away from the field line of entry. At 500 km, r_c (150 keV) ≈ 1 km. At energies of 10 keV and smaller, only about 20% of the particles are charged, and the spreading of these particles is larger than for the higher energy protons.

In Fig. 7 the North–South, and the altitude, distributions of Hα produced by 10 keV protons are shown for various angles between the magnetic field and the vertical. The arc is assumed to be narrow in the North–South direction and long in the East–West direction. The figure shows how the luminosity depends on the magnetic tilt angle. For near vertical incidence the luminosity distribution is symmetric with respect to the magnetic field. When the field is more tilted the luminosity spreads further poleward, consistent with that which was observed for the spreading of the protons seen in Figs 5 and 6.

Keeping the angle between the magnetic field and the vertical constant at $\gamma = 10°$, and considering the energies 10 keV and 100 keV, the spatial distribution of the Hα emission is plotted in Fig. 8. The figure basically reflects the mechanism illustrated in Fig. 1. Low energy protons rapidly become neutralised, with the subsequent change of pitch angles giving rise to a much more extended distribution both in altitude as well as in a North–South direction.

In Fig. 9 the height distribution for the source of escaping ENA is shown for three different initial proton energies, 2, 20 and 100 keV, and an isotropic pitch angle distribution. The interesting double structure at low energies has a simple explanation related to the large differences in the magnitude of the cross sections for electron capture vs recharging. At low projectile energies the protons are neutralised, with a high probability, at much higher altitudes since the capture cross section is large. At the point of electron captures some of the initial protons with pitch angles close to 90° will escape poleward. This first charge exchange and the tilted magnetic field

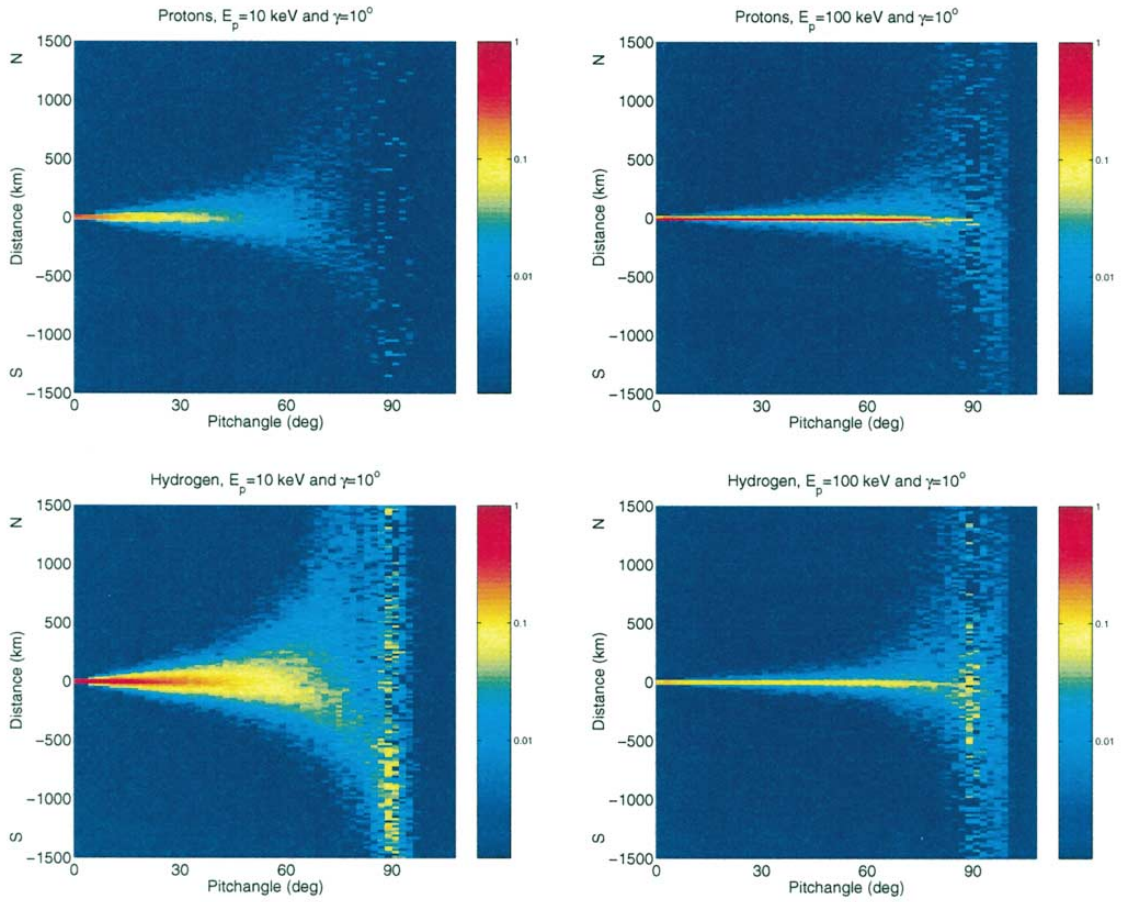

Fig. 6. Pitch angle distribution (erg/cm^3) of protons and hydrogen at 300 km altitude as a function of horizontal distance away from the original (30 km wide) proton arc. The magnetic tilt angle is 10° and two initial proton energies, 10 (mean particle energy at 300 km: 9.7 keV) and 100 keV (mean particle energy at 300 km: 99.5 keV), are considered.

gives rise to the high altitude source for the escaping ENA.

Most of the neutralised particles do, however, continue to propagate downwards. The mean distance for recharging is inversely proportional to the ionisation cross section by the effective N_2 atmosphere. Since this cross section decreases rapidly with energy the mean distance to the next recharging and subsequent change of pitch angles and energies at low energies becomes so large that the ENA source exhibits a double structure. At higher initial energies the distance between the first and second neutralisation process is much smaller. Since the capture cross section is small at high energies, the first neutralisation takes place at low altitudes. Thus the spatial region between the first and higher order neutralisations becomes small, and the two separated mechanisms fall into the same narrow altitude structure.

Table 1 gives the average height for the first charge exchange vs initial proton energy and the magnetic tilt angle γ. It is seen that the average height for the first charge exchange decreases with increasing energy and for more vertical incident of the protons. This is in accordance with what we expect from the cross sections and the altitude dependence of the atmosphere.

Table 1
Average height for first charge exchange (km)

E_P/γ	1°	10°	20°	30°
2 keV	660 km	667 km	652 km	668 km
10 keV	640 km	657 km	616 km	647 km
50 keV	578 km	502 km	519 km	525 km
100 keV	425 km	475 km	329 km	495 km
250 keV	209 km	270 km	274 km	278 km

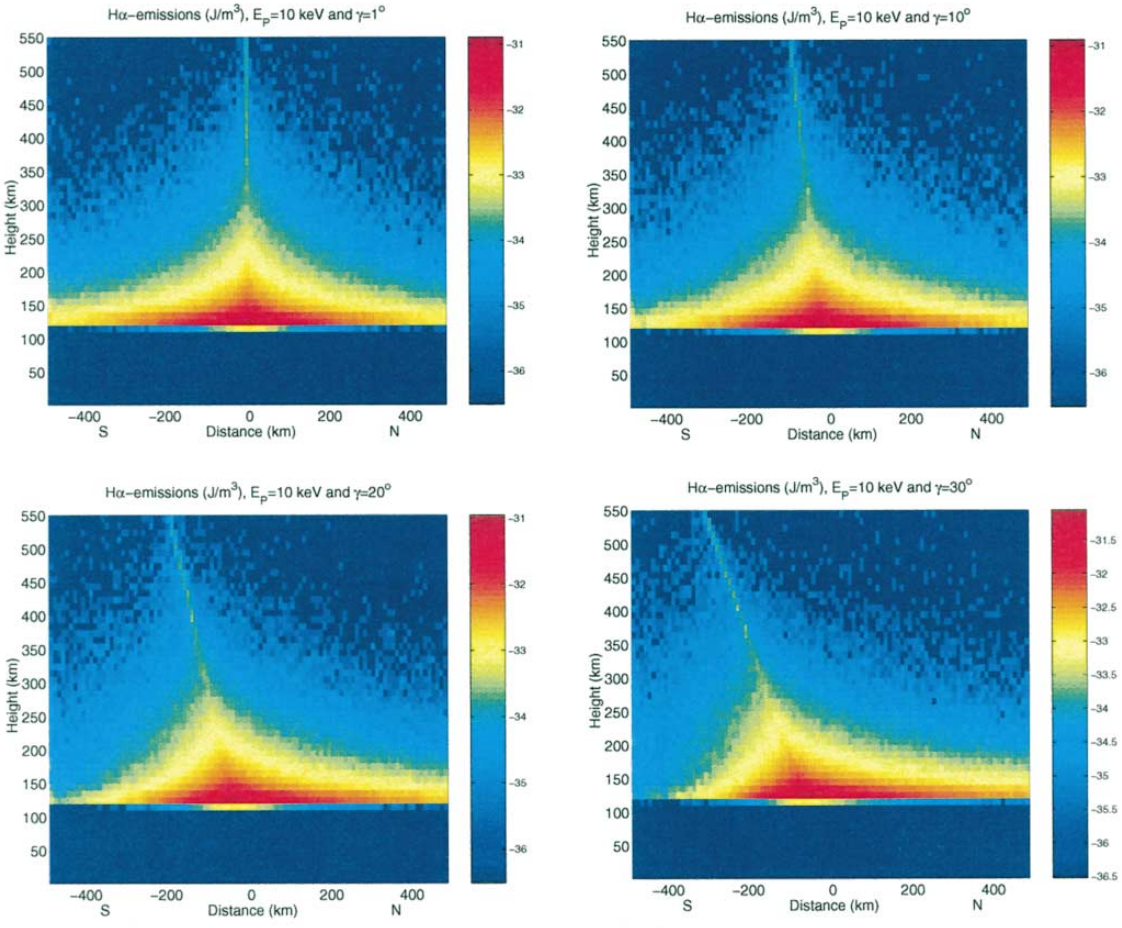

Fig. 7. Horizontal and vertical distribution of Hα emission from 10 keV protons for different magnetic inclinations.

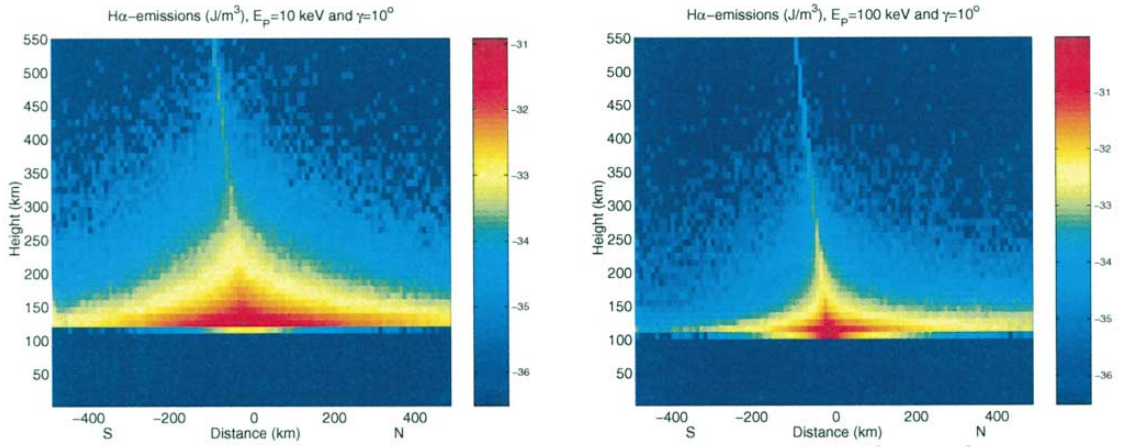

Fig. 8. North–South and altitude distribution of Hα emission for 10 and 100 keV proton energy at a magnetic inclination of 10°.

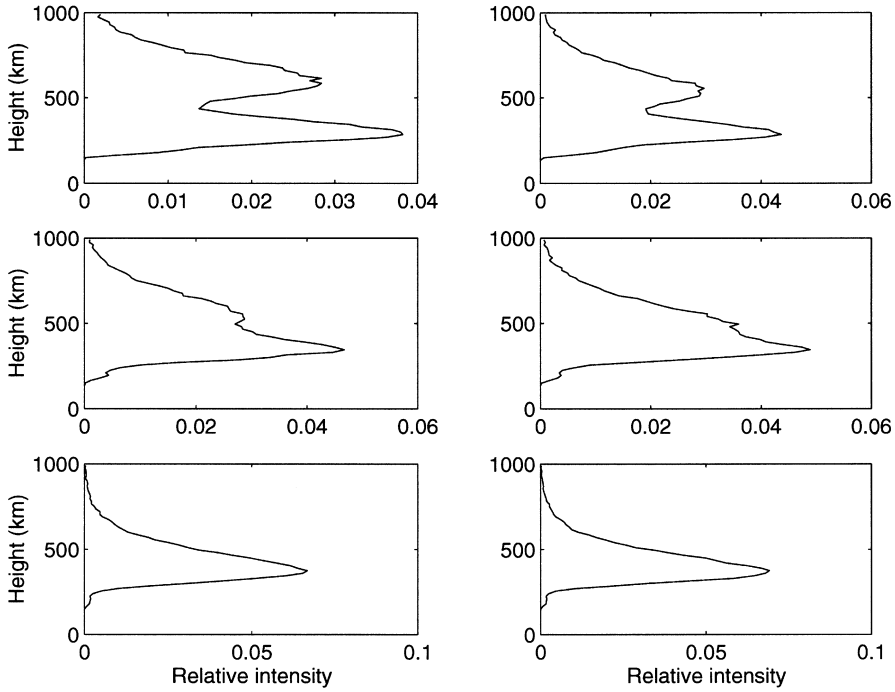

Fig. 9. The altitude dependence for the production of escaping ENA from different proton energies. The magnetic inclination is 10° for the left panels and 20° for the right panels. The initial proton energies are, from top to bottom panel, 2, 20 and 100 keV, and the pitch angle distribution is isotropic in all cases. The mean energy of the escaping ENA is about 85% of the initial energy in all cases.

Table 2
Percentage of scattered particles which mirror and travel back into space along other magnetic field lines, assuming an isotropic pitch angle distribution of the incoming particles

E_P/γ	1°	10°	20°	30°
2 keV	0.1%	0.1%	0.1%	0.1%
10 keV	0.1%	0.2%	0.3%	0.2%
50 keV	0.9%	1.1%	1.2%	1.4%
100 keV	2.5%	2.3%	2.7%	3.5%
250 keV	4.1%	4.1%	4.2%	4.4%

Assuming an isotropic pitch angle distribution of the incoming protons, Table 2 gives the fraction of the protons which mirror and return to the 1000 km altitude after losing some of their energy in the atmosphere. This fraction is fairly insensitive to the magnetic tilt angle, but depends on the energy as the more energetic particles are most likely to survive an encounter with the atmosphere.

In Fig. 10 the fraction of the protons which return from the atmosphere as ENA is plotted. This fraction shows a rather large dependence on both the energy and the magnetic tilt angle. For energies below 20 keV the fraction is rather independent of the energy but increases markedly with the tilt angle, from about 4% for vertical magnetic field to about 16% for a tilt angle of 30°. For higher energies, the flux decreases and, at around 100 keV, the ENA return flux is about 6%, independent of tilt angle.

4. Conclusions

In this paper the altitude distribution of the Hα emission and the flux of ENA returned from the atmosphere have been calculated based on a Monte-Carlo model. The model uses converging magnetic field lines and an effective N_2 atmosphere.

In the energy range below 10 keV about 16% of the incoming proton beam returns as neutrals and at 100 keV about 10% is returned. The latitude and the altitude distribution of Hα is calculated. It is shown that the previously calculated intensities for Hα emission is a factor of about 10 too small. The calculations also give the altitudes for the source of ENA leaving the Earth's atmosphere. A two zone structure for the low energy ENA source can be recognized, with one source of low energy ENA above the main ENA source. These source locations are important when the proton precipitations

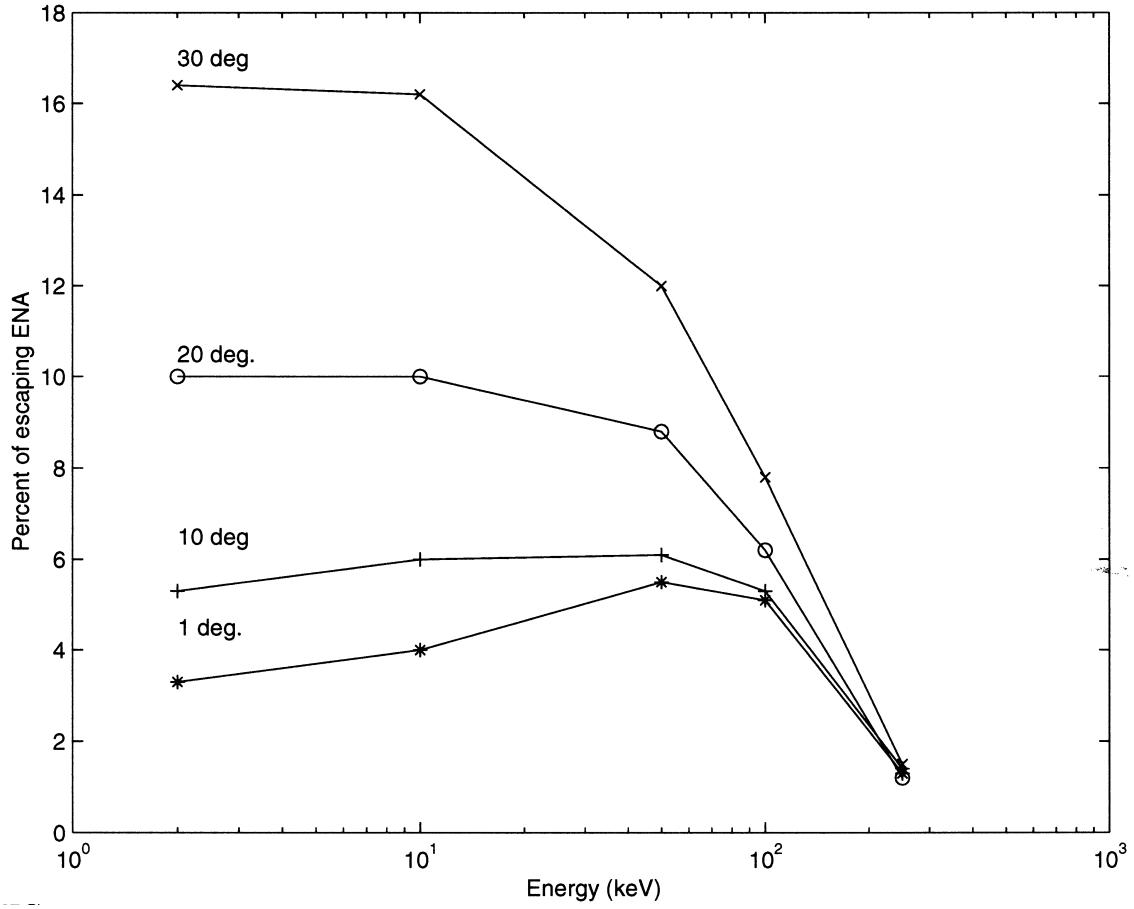

Fig. 10. Percentage of returned ENA as a function of initial proton energy for 4 different tilt angles, 1, 10, 20 and 30°.

are reconstructed from ENA observations. These features will be measured in the future and will provide a sensitive test of the various theoretical models and the collision physics involved.

Acknowledgements

This work has received support from Norges Forskningsråd (NFR) and from the Norwegian Supercomputing Committee (TRU) through a grant of computing time at supercomputing facilities.

References

Andersen, H.H., Zieger, J.F., 1977. The Stopping and Ranges of Ions in Matter. Pergamon.
Chamberlain, J.W., 1954a. Astrophys. J. 120, 360–366.
Chamberlain, J.W., 1954b. Astrophys. J. 120, 566–571.
Chamberlain, J.W., 1957. Astrophys. J. 126, 245–252.
Davidson, T.D., 1965. J. Geophys. Res. 70, 1061–1068.
Davis, L.R., Berg, D.E., Meredith, L.H., 1960. Proceedings of COSPAR Symposium, North Holland, Amsterdam, p. 721.
Decker, D.T., Kozelov, B.V., Basu, B., Jasperse, J.R., 1996. J. Geophys. Res. 101, 26947–26960.
Eather, R.H., Burrows, K.M., 1966. Australian J. Phys. 19, 309–322.
Galand, M., Lilensten, J., Kofman, W., 1997. J. Geophys. Res. 102, 22261–22272.
Gartlein, C.W., 1948. Phys. Rev. 74, 1208.
Gartlein, C.W., 1950. Trans. Am. Geophys. Union 31, 18–20.
Gartlein, C.W., 1951. Phys. Res. 81, 463–464.
Hedin, A.E., 1987. J. Geophys. Res. 92, 4649.
Inglesias, G.E., Vondrak, R.R., 1974. J. Geophys. Res. 79.
Johnstone, A.D., 1972. Planet Space Sci. 20, 292.
Kerby G.W., Gealy, M.W., Hsu, Y.-Y., Rudd, M.E., 1995. Phys. Rev. A 51, 2256.
Koselov, B.V., Yurova, I.Y., 1991. Report PGI-91-3-83. Polar Geophysical Institute, Apatity (in Russian).
Kozelov, B.V., Ivanov, V.E., 1992. Planet. Space Sci. 40, 1503.
Lundblad, J.Å., Søraas, F., Aarsnes, K., 1979. Planet. Space Sci. 27, 841–865.
Meinel, A.B., 1951. Astrophys. J., 113, 50–54.

Norberg et al., 1995. Proceedings of the 12th ESA Symposium on Rocket and Balloon programmes and related research, Lillehammer, Norway, ESA SP-370.
Omholt, A., 1956. J. Atmos. Terr. Phys. 9, 18–27.
Roelof, E.C., Mitchell, D.G., Williams, D.J., 1985. J. Geophys. Res. 90, 10991–11008.
Rudd, M.E., 1979. Phys. Rev. A 20, 787.
Rudd, M.E., Gregorie, D., Crooks, J.B., 1971, Phys. Rev. A 3, 1635.
Rudd, M.E., DuBois, R.D., Toburen, L.H., Ratcliffe, C.A., Goeffe, T.V., 1983. Phys. Rev. A 28, 3244.
Spence, H.E., Blake, J.B., 1997. Adv. Space Res. (in press).
Søraas, F., Lindalen, H.R., Måseide, K., Egeland, A., Sten, T.A., Evans, D.S., 1974. J. Geophys. Res. 79, 1851–1859.
Søraas, F., Aarsnes, K., 1996. Geophys. Res. Lett. 23, 2959–2962.
Synnes, S., 1996. Cand. Scient. thesis, University of Bergen.
Tuan, R.F., 1962. Astophys. J. 136, 283–287.
Toburen, L.H., 1971. Phys. Rev. A 3, 216.
Vegard, L., 1939. Nature 144, 1089–1090.
Vegard, L., 1948. Report of the Gassiot Committee, The Physical Society, London, pp. 82–91.
Yousif, F.B., Geddes, J., Gilbody, H.B., 1986. J. Phys. B 19, 217–231.